

# Performance analysis of OCDMA based underwater data transmission using Li-Fi in LOS/NLOS scenarios

GURLEEN KAUR\*, BALJEET KAUR, GURPURNEET KAUR

*Electronics and Communication Engineering, Guru Nanak Dev Engineering College, Ludhiana, India*

The study investigates Underwater Optical Wireless Communication (UOWC) systems utilizing Optical Code Division Multiple Access (OCDMA) and Li-Fi technology for high-speed underwater data transmission. It evaluates the system performance in Line-of-Sight (LOS) and Non-Line-of-Sight (NLOS) scenarios at data rates of 2.5, 5 and 10 Gigabit per second across various water environments such as 'Pure Sea', 'Clear Ocean', 'Coastal Ocean', 'Harbor I' and 'Harbor II'. Using Diagonal Permutation Shift (DPS) code, the research analyses the impact of water conditions on signal quality and transmission efficiency. Simulations shows that high data rates perform well in clear waters but less effective in turbid harbor conditions. The results confirm successful transmission of a 532 nm signal across five underwater channels and evaluated via Q-factor and eye diagram in NLOS and LOS systems. In the NLOS scenario, the transmission ranges are 38 m, 28 m, 12 m, 8 m, 7 m for NL\_PS, NL\_CL, NL\_CO, NL\_H1, NL\_H2 respectively. In the LOS scenario, the transmission ranges are 50 m, 47 m, 32 m, 17.5 m, 10 m for L\_PS, L\_CL, L\_CO, L\_H1, L\_H2 respectively.

(Received July 31, 2024; accepted February 3, 2025)

**Keywords:** Optical Code Division Multiple Access (OCDMA), Line-of-Sight (LOS), Non-Line-of-Sight (NLOS), Diagonal Permutation Shift (DPS), Underwater Optical Wireless Communication (UOWC), Light Fidelity (Li-Fi)

## 1. Introduction

Underwater communication is crucial for diverse marine applications, including oceanographic research, offshore operations, maritime security and exploration. However, transmitting underwater data is challenging due to factors like signal attenuation and multipath interference. Traditional methods like acoustic and RF communication face limitations such as bandwidth constraints and susceptibility to environmental noise. As a compelling option, Underwater Optical Wireless Communication (UOWC) uses optical signals to deliver higher bandwidth, low latency and greater noise resilience [1,2]. Incorporating technologies like Optical Code Division Multiple Access (OCDMA) enhances both performance and capacity even further. Research focuses on optimizing UOWC systems by studying underwater channel characteristics, modulation techniques, and coding schemes to overcome these challenges [2]. Underwater communication is essential for marine applications, but traditional methods face challenges like signal attenuation. Light Fidelity (Li-Fi), using visible or infrared light, offers high-speed, bidirectional and secure wireless links in air and water. It modulates light intensity to encode digital data, leveraging existing infrastructure for connectivity [2]. Compared to RF, Li-Fi provides higher data rates, lower latency and improved security by confining signals and reducing electromagnetic interference underwater [3-5]. These advantages make Li-Fi promising for reliable data transmission in aquatic environments. RF communication, like Wi-Fi has been predominant for connectivity but faces limitations in underwater environments due to significant signal attenuation and

interference, prompting exploration of alternatives like Li-Fi for more effective data transmission [5].

In past studies, a novel UOWC system had been proposed utilizing OCDMA with Diagonal Permutation Shift (DPS) code using Line-of-sight. The system successfully transmits data at rates of 2.5, 5 and 10 Gigabit per second simultaneously over three channels. The study evaluates system performance for various waterbodies, such as 'Pure Sea (PS)', 'Clear Ocean (CL)', 'Coastal Ocean (CO)', 'Harbor I (HA I)' and 'Harbor II (HA II)' [6]. Performance metrics such as bit error rate (BER), quality factor, and eye diagrams demonstrate successful transmission for ranges of 13 m in PS, 10 m in CL, 7.2 m in CS, 4.3 m in HA I, and 3 m in HA II [6]. The previous work implements Li-Fi technology, transmitting data up to 2-3 meters at 115200 bits per second [7]. It includes a transmitter with components like an ESP 32 module, LED, and MOSFET, and a receiver with a photodiode and amplifier. Li-Fi offers a faster, safer and more eco-friendly alternative to RF communication. Each LED light source can serve as a Li-Fi access point, demonstrating minimal impact on health. Li-Fi has potential applications in airplanes, hospitals, petrochemical industries, smart lighting, and underwater communication. In this work, both Line-of-Sight (LOS) and Non-Line-of-Sight (NLOS) scenarios has been incorporated using Li-Fi technology. While past work focused on LOS communication, this work extends the analysis to address the additional challenges and benefits of NLOS communication [8]. This adds a significant dimension to the performance evaluation in underwater environments, making it more applicable to real-world scenarios where obstacles may impede direct line-of-sight transmission. By comparing and contrasting

the performance metrics such as BER, quality factor and eye diagrams in both LOS and NLOS conditions, the research aims to provide a comprehensive understanding of the potential and limitations of OCDMA based underwater communication systems enhanced with Li-Fi technology.

Overall, the synergistic integration of OCDMA and Li-Fi technologies holds promise for advancing underwater communication capabilities. By leveraging their respective strengths in spectral efficiency, security and robustness to environmental challenges, this approach paves the way for enhanced applications in underwater exploration, environmental monitoring and defense operations [9]. As research continues to evolve, optimizing these technologies will be crucial for meeting the growing demands of underwater communication systems in diverse marine environments [10]. The following is the summary of some major contributions:

- Evaluation of OCDMA based underwater data transmission using Li-Fi in LOS and NLOS scenarios.
- Integration of Li-Fi technology to enhance high-speed communication efficiency underwater.
- Study of system performance parameters across different waterbodies such as 'Pure Sea', 'Clear Ocean', 'Coastal Ocean', 'Harbor I' and 'Harbor II'.

## 2. Basic principles of OCDMA, LOS & NLOS

In underwater wireless communication, the demand for reliable, high capacity and secure data transmission has spurred interest in multiplexing techniques, notably OCDMA [11]. OCDMA allows multiple users to transmit data simultaneously over a shared optical channel using orthogonal codes, unlike traditional methods like Time Division Multiple Access (TDMA) or Wavelength Division (WDMA) [6]. Its unique optical codes ensure effective signal separation and recovery, enhancing spectral efficiency, security and user capacity. OCDMA's inherent security features, utilizing distinct codes for each user, are particularly advantageous in underwater environments where privacy and resilience against eavesdropping are crucial [8]. Researchers explore various OCDMA code families and detection techniques, such as SAC OCDMA with DPS codes, to optimize system performance in challenging underwater conditions. Integrating OCDMA with technologies like Li-Fi and underwater robotics promises to expand the capabilities of underwater optical communication systems, supporting diverse applications in exploration, monitoring, and communication [12]. Combining OCDMA with Li-Fi enhances underwater data transmission by leveraging Li-Fi immunity to electromagnetic interference, high bandwidth, and security features [13-15]. This integration optimizes performance, supporting multiple users with distinct codes over shared optical channels and addressing challenges in underwater communication effectively [16]. The addition of OCDMA and Li-Fi aims to address the limitations of conventional RF communication in underwater

environments, offering enhanced reliability and bandwidth [6]. By utilizing DPS codes for each user, OCDMA provides secure and efficient data transmission, making it highly suitable for applications like underwater exploration, environmental monitoring and defense operations. LOS travel directly from transmitter to receiver without any obstacles in their path. LOS scenarios include direct communication without significant reflections. NLOS refers to where an obstructed path between the transmitter and receiver. In NLOS, multipath propagation occurs due to reflections of surfaces. These reflections create multiple signal paths, affecting signal strength and quality. The range of NLOS communication is shorter than LOS links due to additional losses in reflection and scattering.

While practical considerations, LOS is desirable but not always achievable. NLOS scenarios required specialized methods for transmission and reception. NLOS is essential because it accounts for real world obstacles and enables robust wireless communication. UOWC make use of LOS technology utilizes visible or near infrared light for high speed data transmission between underwater devices like sensors, submarines and autonomous vehicles. It provides benefits such as high bandwidth and minimal latency, overcoming limitations of acoustic and RF methods prone to interference and low data rates [17-19]. In contrast, NLOS UOWC addresses challenges in complex underwater environments by employing techniques that navigate around obstacles using signal reflections, scattering, and diffraction, ensuring reliable data transfer where direct paths are obstructed. The research focuses on evaluating OCDMA based underwater data transmission in both LOS and NLOS scenarios. LOS UOWC leverages direct optical paths between transmitters and receivers [20]. On the other hand, NLOS UOWC system addresses complex practical underwater environment such as obstacles, variable terrain, and high turbidity by using water-air surface, seabed and walls which increases the likelihood reception of reflected signal. Techniques such as signal reflections, scattering and diffraction are employed to ensure reliable data transmission in these challenging conditions [21,22]. UOWC employs LOS and NLOS configurations to facilitate high speed data transmission. LOS utilizes direct optical paths between transmitter and receiver, while NLOS techniques navigate around obstacles using reflections and diffraction, suitable for complex underwater environments. OCDMA enhances system capacity by allowing multiple users to share the same optical channel using unique codes. The study assesses system performance using the Q-factor metric across different types of waterbodies, including 'Pure Sea', 'Clear Ocean', 'Coastal Ocean', 'Harbor I' and 'Harbor II'. It examines how water characteristics like turbidity and environmental conditions impact signal quality and transmission efficiency.

### 3. Layout of proposed UOWC system employing OCDMA DPS code

The proposed UOWC system uses OCDMA and DPS coding. The transmitter section, generates data rates of 2.5, 5 and 10 Gigabit per second using a pseudo-random bit sequence generator, NRZ encoding and six Lasers.

The all six lasers are multiplexed to create a single channel, then the output of the multiplexer goes to the MZ modulator as shown in Fig. 1(a). Similarly, all five channels has been created. In the receiver section, firstly signal goes to the amplifier then the amplified signal is applied to fibre bragg grating, which operates at the same wavelength as the lasers. After additional processing involving s-decoder, combiner, optical subtractor, photodiode and low pass filter components. Finally, analyse the signal using BER analyser to obtain the results as outlined in Fig. 1(b).

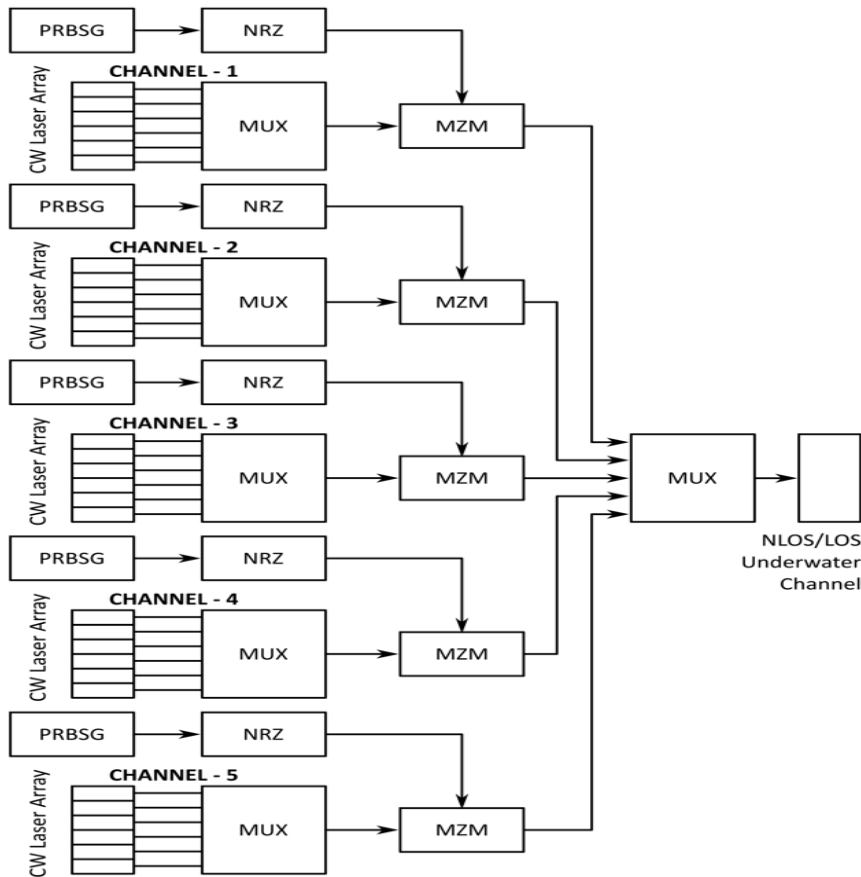
The UOWC system effectively combines OCDMA and DPS coding to achieve high data rates and reliable signal detection, utilizing NRZ format transmission, FBG based decoders and SPDs for efficient channel separation and decoding.

In UOWC, the selection of the wavelength is critical since different wavelength of light experience varying degrees of absorption and scattering in water. In this work, 532 nm (green light) wavelength was selected to avoid channel attenuation and to improve the efficiency of system. Some of these are discussed below:

**1. Low absorption rate:** Water absorbs EM waves differently based on wavelength. Blue-Green wavelengths (450 nm-550 nm) experience minimal absorption compared to other like UV or IR. In clear water green light can travel several metres before being significantly attenuated making it ideal for underwater communication.

**2. Reduced scattering:** The scattering affects all optical signals which travel underwater. The green light wavelength scatters less as compared to blue wavelength (around 450 nm). This balance between low absorption and manageable scattering makes green light an efficient choice.

**3. Suitability for clear and turbid waters:** Green light offers better penetration than both longer (red/IR) and shorter (blue/UV) wavelengths in both clear and moderately turbid waters, making it adaptable for various underwater environments.



(a) Transmitter

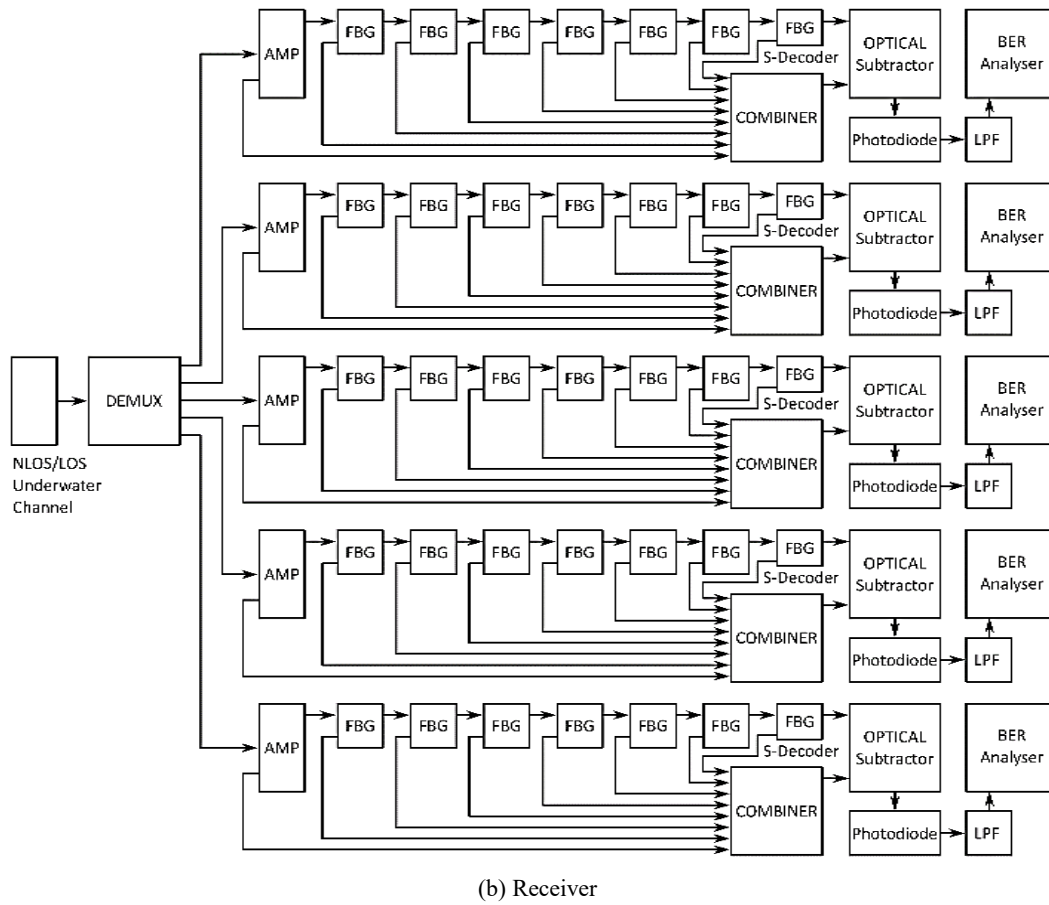


Fig. 1. UOWC system utilizing OCDMA/DPS code (a) Transmitter (b) Receiver

**4. Low power consumption:** The wavelength of 532 nm travels longer distance without excessive power consumption since less energy is lost through absorption. Additionally this wavelength supports higher data rates compared to acoustic or radio signals, which are commonly used underwater but limited in bandwidth.

**5. Environmental Safety:** Green light at 532 nm is non-ionizing and harmless to marine life, making it a safer choice than UV light for long-term deployment.

Therefore, channel attenuation plays a critical role in underwater optical wireless communication (UOWC) systems, as it directly impacts the strength and quality of the transmitted signal.

### 3.1. DPS code generation

The DPS code is constructed used in OCDMA systems. The purpose and importance of DPS code is Multiple Access Interference (MAI), it's significant issue in OCDMA systems. It arises when multiple users transmit data simultaneously which causing interference. The DPS code is designed to mitigate the MAI. DPS codes are deprived from well known prime codes and perform certain matrix operations. The DPS code enhance the system's performance by reducing interference and noise, making them valuable for high speed networks [2].

This section describes the construction of DPS codes for OCDMA. These codes are similar to other OCDMA codes, are characterized by parameters including 'code weight ( $C_w$ )', 'No. of channels ( $N_c$ )' and 'code length ( $L_c$ )' [6]. The output fields are expressed in the following equations (1-11).

Usually,  $C_w$  is selected as a prime number which is always greater than 2, and  $N_c$  is correlative to  $C_w$ .

$$N_c = C_w^2 \quad (1)$$

Additionally,  $L_c$  can be characterized relative to both  $N$  and  $C_w$  as:

$$L_c = N_c + C_w \quad (2)$$

To create the DPS code sequence, when  $C_w = 5$  the following four sequential processes must be obtained such as Diagonal, Permutation, Shifting and Joining. The detail of each process is explained as:

#### Step I: Diagonal process

Create a primary diagonal sequence ( $x_{0,0}$ ) and generator sequence ( $X_5$ ) as given below:

$$x_{0,0} = (0 \times 0) \bmod \quad (3)$$

$$X_5 = [X_{(0,0)}, X_{(1,1)}, X_{(2,2)}, X_{(3,3)}, X_{(4,4)}] \quad (4)$$

### Step II: Permutation process

In this process, a  $5 \times 5$  basic matrix ( $Q_5^0$ ) is constructed by taking the same components of  $X_5$  in 1<sup>st</sup> row then generate the remaining row components with the help of permutation process. The permutation process is applied one time in all consecutive rows so that a symmetric matrix with zero diagonal values can be generated without repetition.

$$Q_5^0 = \begin{bmatrix} 0 & 0 & 1 & 0 & 1 \\ 0 & 0 & 0 & 1 & 0 \\ 0 & 1 & 0 & 0 & 1 \\ 1 & 0 & 1 & 0 & 1 \\ 0 & 1 & 0 & 1 & 0 \end{bmatrix} \quad (5)$$

### Step III: Shifting process

In this procedure, four new matrices namely,  $Q_5^1$ ,  $Q_5^2$ ,  $Q_5^3$  and  $Q_5^4$  are constructed using shifting process. To set up the matrix  $Q_5^1$  an integer value '1' is added to every component in  $Q_5^0$  and simultaneously apply modulo 5 in the resultant matrix.

$$Q_5^1 = \begin{bmatrix} (0+1) \bmod 5 & (0+1) \bmod 5 & (1+1) \bmod 5 & (0+1) \bmod 5 & (1+1) \bmod 5 \\ (1+1) \bmod 5 & (0+1) \bmod 5 & (0+1) \bmod 5 & (1+1) \bmod 5 & (0+1) \bmod 5 \\ (0+1) \bmod 5 & (1+1) \bmod 5 & (0+1) \bmod 5 & (0+1) \bmod 5 & (1+1) \bmod 5 \\ (1+1) \bmod 5 & (0+1) \bmod 5 & (1+1) \bmod 5 & (0+1) \bmod 5 & (0+1) \bmod 5 \\ (0+1) \bmod 5 & (1+1) \bmod 5 & (0+1) \bmod 5 & (1+1) \bmod 5 & (0+1) \bmod 5 \end{bmatrix}$$

$$Q_5^1 = \begin{bmatrix} 1 & 1 & 2 & 1 & 2 \\ 2 & 1 & 1 & 2 & 1 \\ 1 & 2 & 1 & 1 & 2 \\ 2 & 1 & 2 & 1 & 1 \\ 1 & 2 & 1 & 2 & 1 \end{bmatrix} \quad (6)$$

While for the matrix  $Q_5^2$ , each element is incremented by a value of 2 in  $Q_5^0$  matrix, then perform modulo 5 in the result as:

$$Q_5^2 = \begin{bmatrix} (0+2) \bmod 5 & (0+2) \bmod 5 & (1+2) \bmod 5 & (0+2) \bmod 5 & (1+2) \bmod 5 \\ (1+2) \bmod 5 & (0+2) \bmod 5 & (0+2) \bmod 5 & (1+2) \bmod 5 & (0+2) \bmod 5 \\ (0+2) \bmod 5 & (1+2) \bmod 5 & (0+2) \bmod 5 & (0+2) \bmod 5 & (1+2) \bmod 5 \\ (1+2) \bmod 5 & (0+2) \bmod 5 & (1+2) \bmod 5 & (0+2) \bmod 5 & (0+2) \bmod 5 \\ (0+2) \bmod 5 & (1+2) \bmod 5 & (0+2) \bmod 5 & (1+2) \bmod 5 & (0+2) \bmod 5 \end{bmatrix}$$

$$Q_5^2 = \begin{bmatrix} 2 & 2 & 3 & 2 & 3 \\ 3 & 2 & 2 & 3 & 2 \\ 2 & 3 & 2 & 2 & 3 \\ 3 & 2 & 3 & 2 & 2 \\ 2 & 3 & 2 & 3 & 2 \end{bmatrix} \quad (7)$$

Similarly, for matrix  $Q_5^3$ , each element is incremented by a value of 3 in  $Q_5^0$  matrix, then perform modulo 5 in the result as mentioned in eq.(8).

$$Q_5^3 = \begin{bmatrix} (0+3) \bmod 5 & (0+3) \bmod 5 & (1+3) \bmod 5 & (0+3) \bmod 5 & (1+3) \bmod 5 \\ (1+3) \bmod 5 & (0+3) \bmod 5 & (0+3) \bmod 5 & (1+3) \bmod 5 & (0+3) \bmod 5 \\ (0+3) \bmod 5 & (1+3) \bmod 5 & (0+3) \bmod 5 & (0+3) \bmod 5 & (1+3) \bmod 5 \\ (1+3) \bmod 5 & (0+3) \bmod 5 & (1+3) \bmod 5 & (0+3) \bmod 5 & (0+3) \bmod 5 \\ (0+3) \bmod 5 & (1+3) \bmod 5 & (0+3) \bmod 5 & (1+3) \bmod 5 & (0+3) \bmod 5 \end{bmatrix}$$

$$Q_5^3 = \begin{bmatrix} 3 & 3 & 4 & 3 & 4 \\ 4 & 3 & 3 & 4 & 3 \\ 3 & 4 & 3 & 3 & 4 \\ 4 & 3 & 4 & 3 & 3 \\ 3 & 4 & 3 & 4 & 4 \end{bmatrix} \quad (8)$$

While for the matrix  $Q_5^4$ , each element is incremented by a value of 4 in  $Q_5^0$  matrix, similarly then perform modulo 5 in the result as expressed in eq.(9).

$$Q_5^4 = \begin{bmatrix} (0+4) \bmod 5 & (0+4) \bmod 5 & (1+4) \bmod 5 & (0+4) \bmod 5 & (1+4) \bmod 5 \\ (1+4) \bmod 5 & (0+4) \bmod 5 & (0+4) \bmod 5 & (1+4) \bmod 5 & (0+4) \bmod 5 \\ (0+4) \bmod 5 & (1+4) \bmod 5 & (0+4) \bmod 5 & (0+4) \bmod 5 & (1+4) \bmod 5 \\ (1+4) \bmod 5 & (0+4) \bmod 5 & (1+4) \bmod 5 & (0+4) \bmod 5 & (0+4) \bmod 5 \\ (0+4) \bmod 5 & (1+4) \bmod 5 & (0+4) \bmod 5 & (1+4) \bmod 5 & (0+4) \bmod 5 \end{bmatrix}$$

$$Q_5^4 = \begin{bmatrix} 4 & 4 & 0 & 4 & 0 \\ 0 & 4 & 4 & 0 & 4 \\ 4 & 0 & 4 & 4 & 0 \\ 0 & 4 & 0 & 4 & 4 \\ 4 & 0 & 4 & 0 & 4 \end{bmatrix} \quad (9)$$

### Step IV: Joining process

In the joining method, an additional column 'E' is added to each of the matrices  $Q_5^0$ ,  $Q_5^1$ ,  $Q_5^2$ ,  $Q_5^3$  and  $Q_5^4$  matrices, Where 'E' is a matrix of size  $5 \times 1$  with components  $\{0;1;2;3;4\}$ . Then all five matrices mentioned in eq.(5), eq.(6), eq.(7), eq.(8) and eq.(9) including 'E' matrix are combined together to make the DPS matrix as:

$$M_{DPS} = \begin{bmatrix} 0 & 0 & 1 & 0 & 1 & 0 \\ 1 & 0 & 0 & 1 & 0 & 1 \\ 0 & 1 & 0 & 0 & 1 & 2 \\ 1 & 0 & 1 & 0 & 0 & 3 \\ 0 & 1 & 0 & 1 & 0 & 4 \\ 1 & 1 & 2 & 1 & 2 & 0 \\ 2 & 1 & 1 & 2 & 1 & 1 \\ 1 & 2 & 1 & 1 & 2 & 2 \\ 2 & 1 & 2 & 1 & 1 & 2 \\ 1 & 2 & 1 & 2 & 1 & 4 \\ 2 & 2 & 3 & 2 & 3 & 0 \\ 3 & 2 & 2 & 3 & 2 & 1 \\ 2 & 3 & 2 & 2 & 3 & 2 \\ 3 & 2 & 3 & 2 & 2 & 3 \\ 2 & 3 & 2 & 3 & 2 & 4 \\ 3 & 3 & 4 & 3 & 4 & 0 \\ 4 & 3 & 3 & 4 & 3 & 1 \\ 3 & 4 & 3 & 2 & 4 & 2 \\ 4 & 3 & 4 & 3 & 3 & 3 \\ 3 & 4 & 3 & 4 & 3 & 4 \\ 4 & 4 & 0 & 4 & 0 & 0 \\ 0 & 4 & 4 & 0 & 4 & 1 \\ 4 & 0 & 4 & 4 & 0 & 2 \\ 0 & 4 & 0 & 4 & 4 & 3 \\ 4 & 0 & 4 & 0 & 4 & 4 \end{bmatrix} \quad (10)$$

Furthermore, to generate code sequences corresponding to each individual row within the matrix  $M_D$ , substitute "0" with the code "10000," "1" with "01000," "2" with "00100," "3" with "00010." and "4"

with "00001." The resultant matrix shown in eq. (11) is the DPS code sequences matrix.

$$M_{DPS} = \begin{bmatrix} 10000 & 10000 & 01000 & 10000 & 01000 & 10000 \\ 01000 & 10000 & 10000 & 01000 & 10000 & 01000 \\ 10000 & 01000 & 10000 & 10000 & 01000 & 00100 \\ 01000 & 10000 & 01000 & 10000 & 10000 & 00010 \\ 10000 & 01000 & 10000 & 01000 & 10000 & 00001 \\ 01000 & 01000 & 00100 & 01000 & 00100 & 10000 \end{bmatrix} \quad (11)$$

Table 1 shows the DPS code sequence generated for wavelengths ranging from 532 nm to 544 nm. It is observed that every wavelength gets a unique code. These codes are generated by four different processes i.e. diagonal, permutation, shifting, and joining.

Table 1. DPS code sequence for different wavelengths in nm scale

532.0	532.8	533.6	534.4	535.2	536	536.8	537.6	538.4	539.2	540	540.8	541.6	542.4	543.2	544
1	0	0	0	0	1	0	0	0	0	0	1	0	0	0	1
0	1	0	0	0	1	0	0	0	0	1	0	0	0	0	0
1	0	0	0	0	0	1	0	0	0	1	0	0	0	0	1
0	1	0	0	0	1	0	0	0	0	0	1	0	0	0	1
1	0	0	0	0	0	1	0	0	0	1	0	0	0	0	0
	1	0	0	0	0	1	0	0	0	0	0	1	0	0	0

#### 4. Stimulation and results of OCDMA based underwater data transmission using Li-Fi

The proposed system, using OCDMA DPS codes, was simulated at data rates of 2.5, 5 and 10 Gigabit per second per channel with a transmitted power of 15 dBm using OptiSystem software. The simulation covered different waterbodies such as 'Non-Line-of-Sight\_Pure Sea (NL\_PS)', 'Non-Line-of-Sight\_Clear Ocean (NL\_CL)', 'Non-Line-of-Sight\_Coastal Ocean (NL\_CO)', 'Non-Line-of-Sight\_Harbor 1 (NL\_H1)', 'Non-Line-of-Sight\_Harbor 2 (NL\_H2)', and 'Line-of-Sight\_Pure Sea (L\_PS)', 'Line-of-Sight\_Clear Ocean (L\_CL)', 'Line-of-Sight\_Coastal Ocean (L\_CO)', 'Non-Line-of-Sight\_Harbor 1 (L\_H1)', 'Non-Line-of-Sight\_Harbor 2 (L\_H2)', conditions. The system's performance was evaluated through eye diagrams and Q-factor measurements, providing insights into communication quality and reliability. Eye diagram depict signal clarity and noise levels, while the Q-factor indicates signal quality and bit error rate (BER) performance. These metrics help to assess the system's feasibility and efficiency in different environments at variable data rates. The following subsections present detailed results and implications for each water body and communication scenario.

#### 4.1. Performance investigation based on Q-Factor for single channel

In this section, the Q-factor analysis evaluates the system's performance for NL\_PS, NL\_CL, NL\_CO, NL\_H1, NL\_H2 and L\_PS, L\_CL, L\_CO, L\_H1, L\_H2 waterbodies at 2.5, 5 and 10 Gigabit per second data rates for single channel. It is examined that, the Q-factor provides valuable insights into the performance of the OCDMA based underwater Li-Fi system. The required value of Q-factor for successful communication is 6(minimum). Tables 2 and 3 demonstrates the Q-Factor values greater than 6. Such findings are pivotal for optimizing system parameters and enhancing the reliability of underwater optical communication, thereby supporting its feasibility and effectiveness in real world applications [6,8].

Table 2 express the LOS Q-Factor for the UOWC system using OCDMA DPS code at 50 m for LOS\_PS, 47 m for L\_CL, 32 m for L\_CO, 17.5 m for L\_H1 and 10 m for L\_H2 using 2.5, 5 and 10 Gigabit per second data rates. Table 3 demonstrates the NLOS Q-Factor for the UOWC system using OCDMA DPS code at 38 m for NL\_PS, 28 m for NL\_CL, 12 m for NL\_CO, 8 m for NL\_H1 and 7 m for NL\_H2 using 2.5, 5 and 10 Gigabit per second data rates.

Table 2. LOS Q – Factor for different waterbodies using different data rates

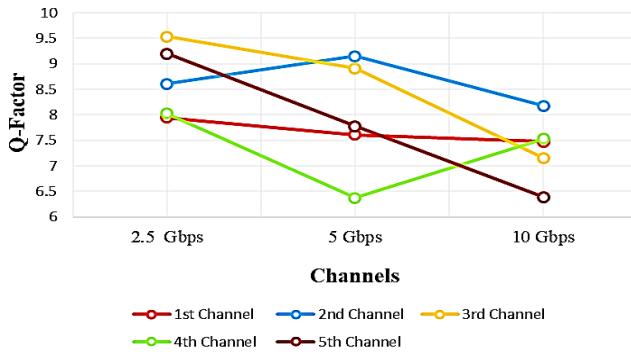
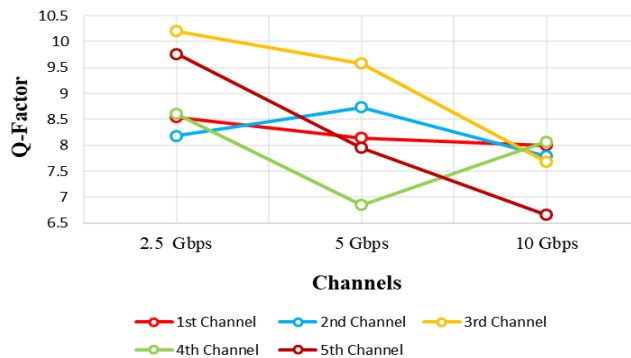
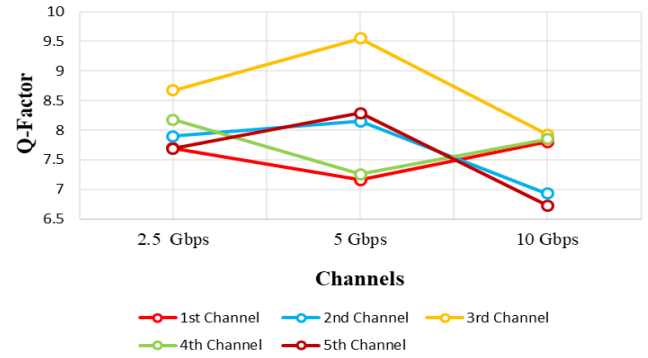
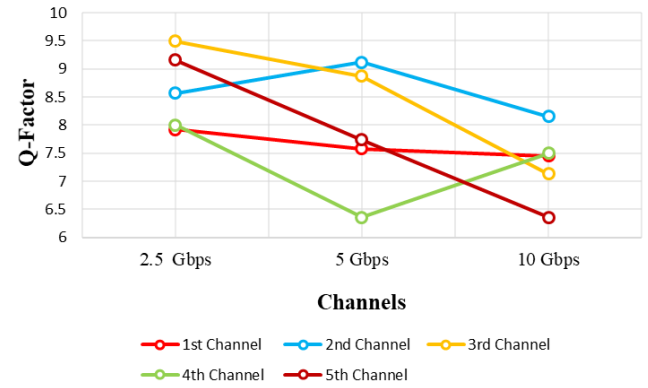
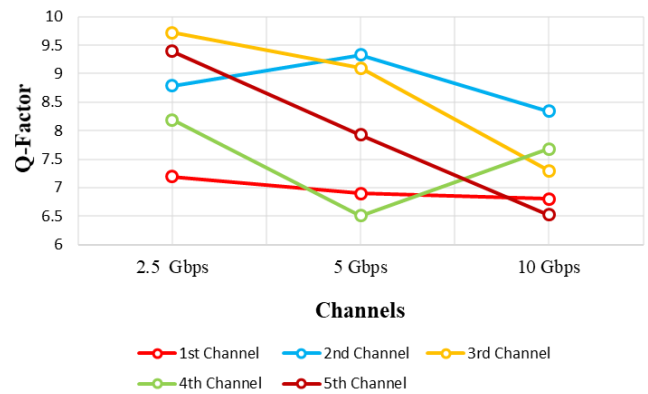
WATER TYPES & LENGTH →	L_PS (50 m)	L_CL (47 m)	L_CO (32 m)	L_H1 (17.5 m)	L_H2 (10 m)
DATA RATE ↓					
2.5 Gbps	8.61	8.18	7.90	8.57	8.79
5 Gbps	9.15	8.73	8.15	9.12	9.33
10 Gbps	8.18	7.79	6.93	8.15	8.34

Table 3. NLOS Q-Factor for different waterbodies using different data rates

WATER TYPES & LENGTH →	NL_PS (38 m)	NL_CL (28 m)	NL_CO (12 m)	NL_H1 (8 m)	NL_H2 (7 m)
DATA RATE ↓					
2.5 Gbps	8.35	8.79	8.00	9.38	9.11
5 Gbps	9.15	9.34	7.81	8.56	8.30
10 Gbps	8.42	8.35	9.05	8.39	8.15

#### 4.2. Performance investigation based on Q-Factor for multiple channels

This section evaluates the Q-Factor performance of UOWC systems for multiple channels. Specifically, the study investigates the application of OCDMA and DPS coding techniques in enhancing communication reliability and efficiency underwater. Through comprehensive analysis and graphical representation, this study aims to provide insights into the effectiveness of these coding methods in UOWC scenarios. The Q-Factor performance for multiple channels is illustrated in the form of graphs in Figs. 2-11 under various conditions.


 Fig. 2.  $L_{PS}$  Q-Factor for OCDMA based UOWC using Li-Fi for different channels and data rates (colour online)

 Fig. 3.  $L_{CL}$  Q-Factor for OCDMA based UOWC using Li-Fi for different channels and data rates (colour online)

 Fig. 4.  $L_{CO}$  Q-Factor for OCDMA based UOWC using Li-Fi for different channels and data rates (colour online)

 Fig. 5.  $L_{H1}$  Q-Factor for OCDMA based UOWC using Li-Fi for different channels and data rates (colour online)

 Fig. 6.  $L_{H2}$  Q-Factor for OCDMA based UOWC using Li-Fi for different channels and data rates (colour online)

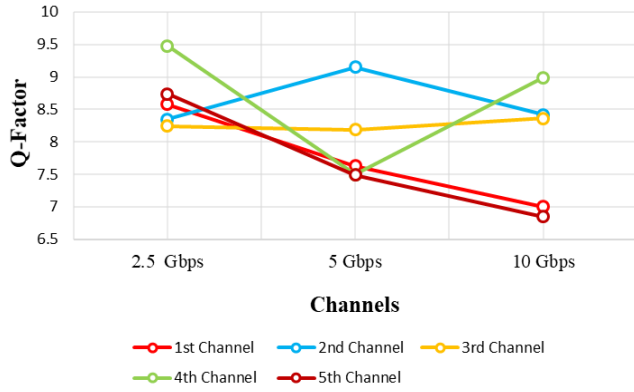


Fig. 7. NL\_PS Q-Factor for OCDMA based UOWC using Li-Fi for different channels and data rates (colour online)

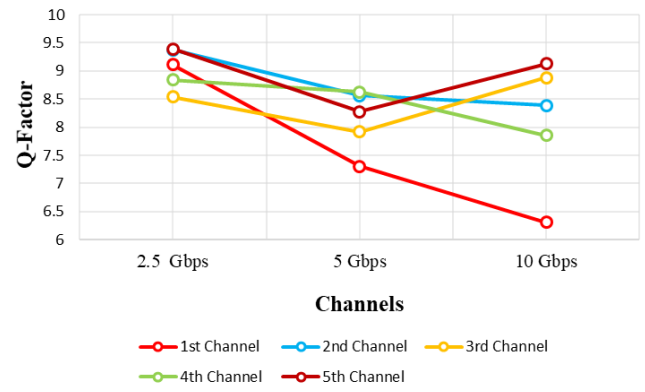


Fig. 10. NL\_H1 Q-Factor for OCDMA based UOWC using Li-Fi for different channels and data rates (colour online)

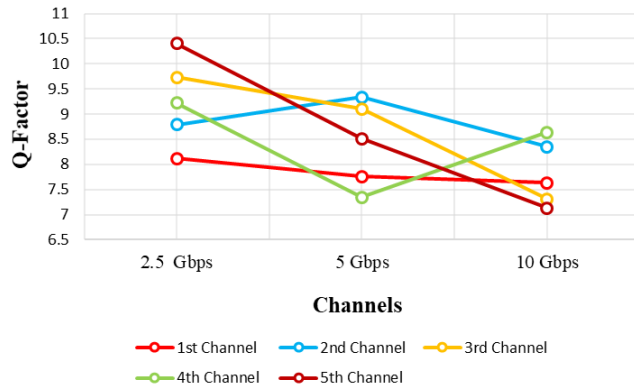


Fig. 8. NL\_CL Q-Factor for OCDMA based UOWC using Li-Fi for different channels and data rates (colour online)

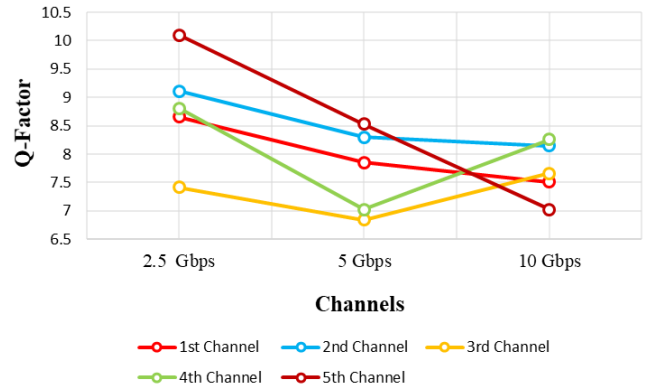


Fig. 11. NL\_H2 Q-Factor for OCDMA based UOWC using Li-Fi for different channels and data rates (colour online)

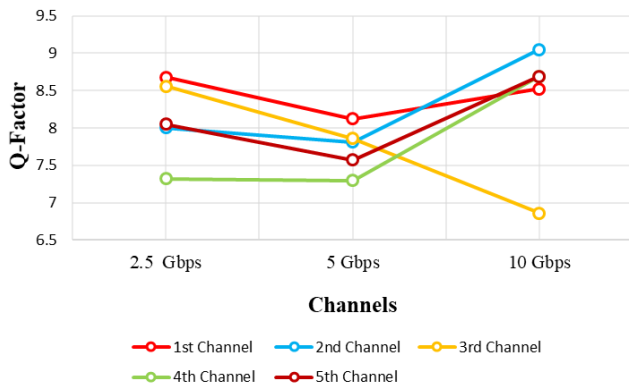


Fig. 9. NL\_CO Q-Factor for OCDMA based UOWC using Li-Fi for different channels and data rates (colour online)

These graphs provide a detailed view of how the Q-factor varies with data rates and environmental conditions, offering critical insights into the reliability and efficiency of OCDMA/DPS coding techniques in UOWC systems.

### 4.3. Performance investigation based on eye diagram for single channel

Eye diagrams serve as a common metric for evaluating the quality of received signals. An eye diagram also known as an eye pattern, is a graphical representation where the signal waveform is plotted over multiple periods. The x-axis represents time and the y-axis represents amplitude. The quality of signal is calculated by widening of an eye opening in an eye diagram. Therefore, greater is the opening of an eye and larger is the signal strength with decreased BER [6].

The performance evaluation of OCDMA based underwater Li-Fi system for L\_PS, L\_CL, L\_CO, L\_H1, L\_H2 and NL\_PS, NL\_CL, NL\_CO, NL\_H1, NL\_H2 has been done in this section using eye diagram for single channel. The eye diagrams shown in Figs. 12-21 illustrate the signal characteristics under LOS and NLOS conditions across different waterbodies and data rates. Each diagram

represents the clarity and stability of transmitted signals, crucial for assessing system reliability in challenging underwater scenarios.

Fig. 12 shows the eye diagrams for the designed UOWC OCDMA based Li-Fi system in L\_PS water type for a underwater range of 50 m, demonstrating different data rates. Fig. 13 represents the eye diagram for L\_CL water type with underwater distance 47 m at different data rates. In addition, Fig. 14 outlines the eye diagrams at an underwater range of 32 m for L\_CO water type, taking data rates of 2.5, 5 and 10 Gigabit per second. Furthermore, Fig. 15 outlines the eye diagrams for L\_H1 at 17.5 m for different data rates. Correspondingly, Fig. 16 describe the eye diagram for L\_H2 at 10 m for various data rates.

Similarly, the eye diagrams for different waterbodies using NLOS scenario are outlined in Figs. 17-21. Fig. 17 outlines the eye diagrams for the proposed UOWC-

OCDMA based Li-Fi system in NL\_PS water type for a range of 38 m, demonstrating different data rates. Fig. 18 represents the eye diagrams for NL\_CL water type with a underwater span of 28 m at different data rates. In addition, Fig. 19 outlines the eye diagrams at an underwater range of 12 m for NL\_CO water type, taking data rates of 2.5, 5 and 10 Gigabit per second. Furthermore, Fig. 20 outlines the eye diagrams for NL\_H1 at 8 m for different data rates. Correspondingly, Fig. 21 describe the eye diagram for NL\_H2 at 7 m for various data rates.

The broad eye openings outlined in Figs. 12–21 prove that all signal information is transmitted and received properly. The red line shown in all eye diagrams depicts the signal transmission over time. In numerous digital communication systems, signal sampling decisions occur at the bit interval's midpoint [6].

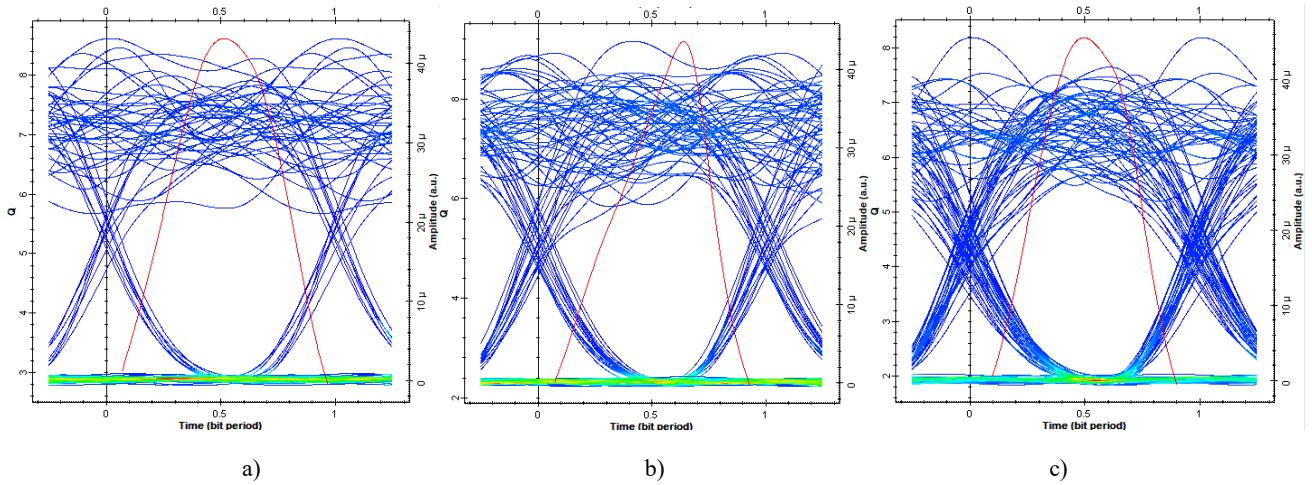


Fig. 12. Eye diagram for L\_PS at a distance of 50 m varies across different data rates (a) 2.5 Gigabit per second (b) 5 Gigabit per second (c) 10 Gigabit per second (colour online)

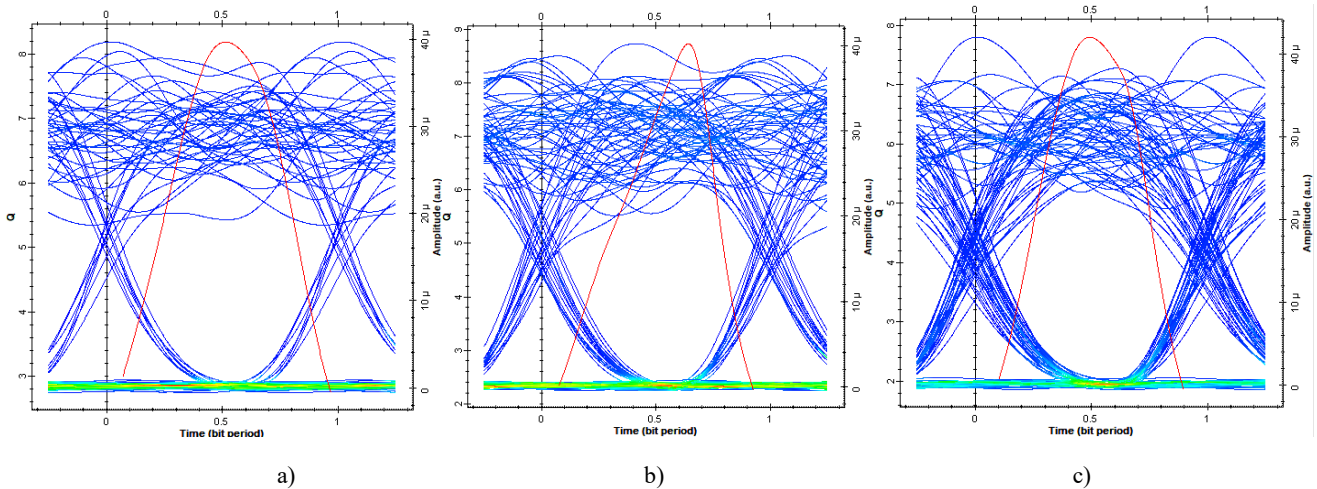


Fig. 13. Eye diagram for L\_CL at a distance of 50 m varies across different data rates (a) 2.5 Gigabit per second (b) 5 Gigabit per second (c) 10 Gigabit per second (colour online)

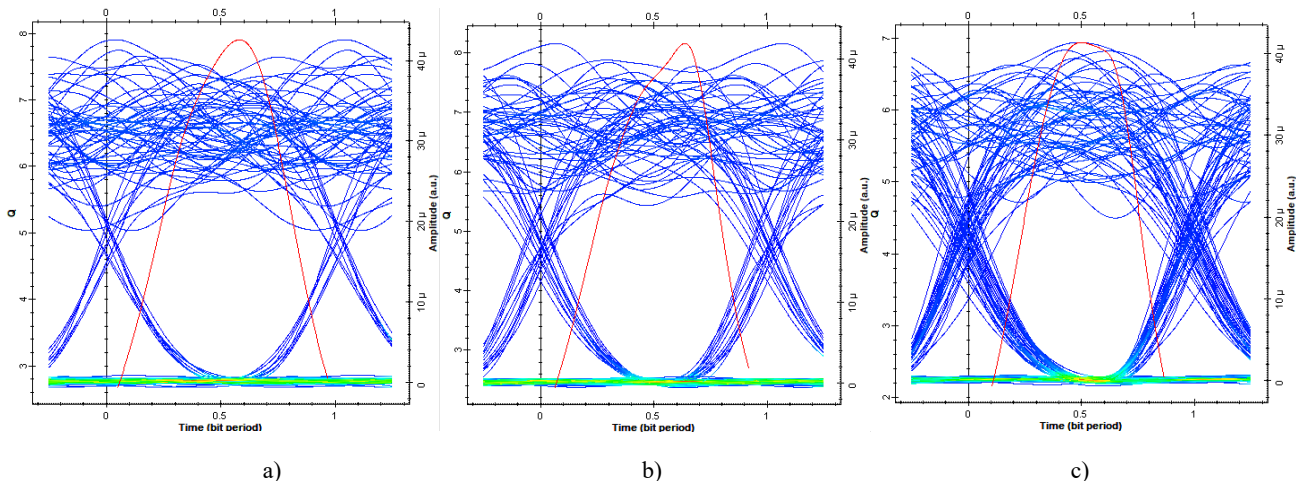


Fig. 14. Eye diagram for  $L_{CO}$  at a distance of 50 m varies across different data rates (a) 2.5 Gigabit per second (b) 5 Gigabit per second (c) 10 Gigabit per second (colour online)

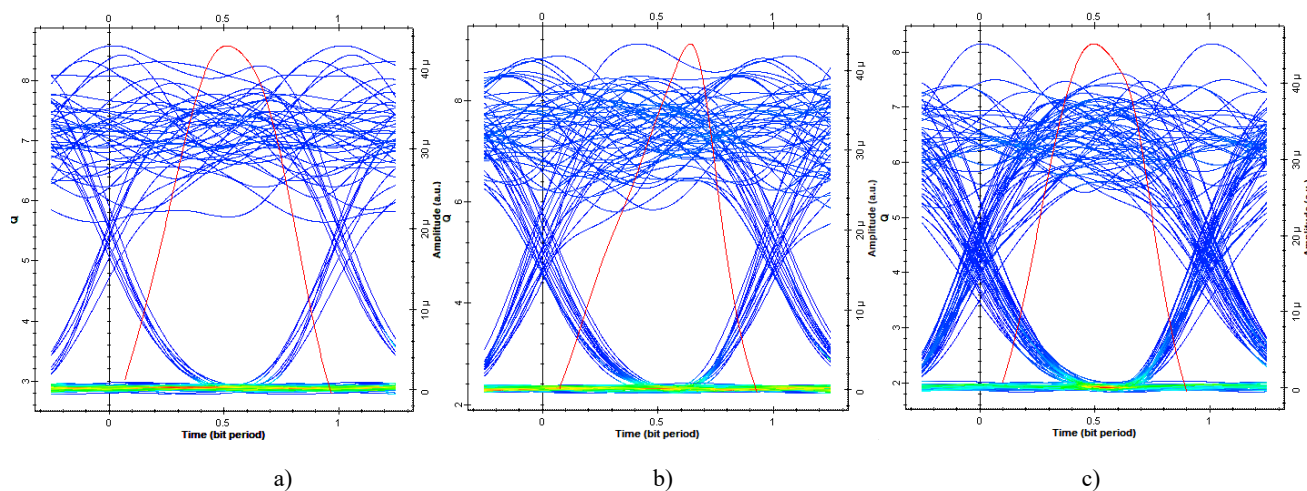


Fig. 15. Eye diagram for  $L_{H1}$  at a distance of 50 m varies across different data rates (a) 2.5 Gigabit per second (b) 5 Gigabit per second (c) 10 Gigabit per second (colour online)

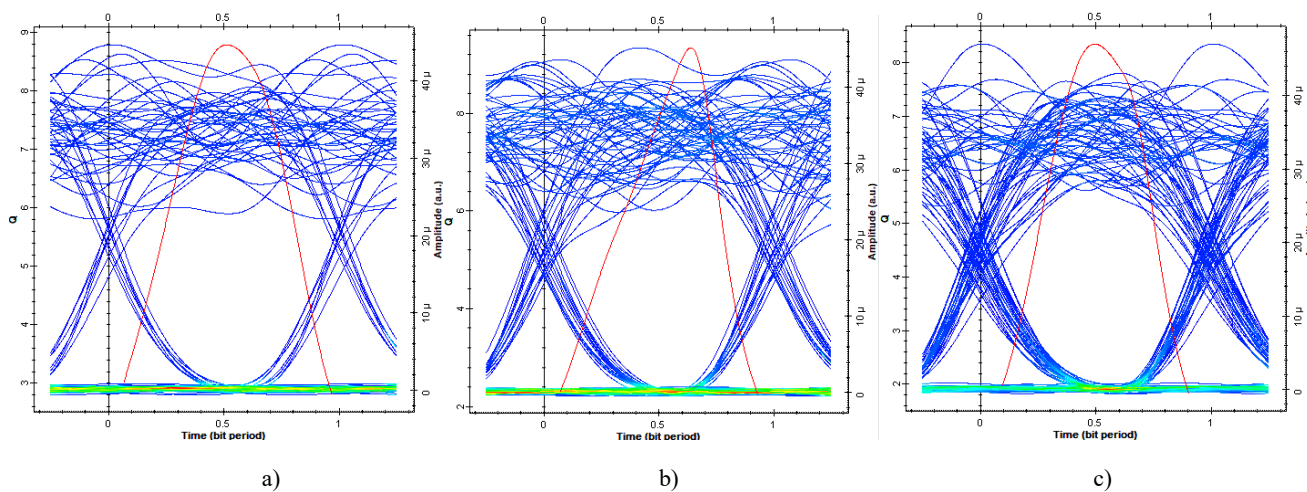


Fig. 16. Eye diagram for  $L_{H2}$  at a distance of 50 m varies across different data rates (a) 2.5 Gigabit per second (b) 5 Gigabit per second (c) 10 Gigabit per second (colour online)

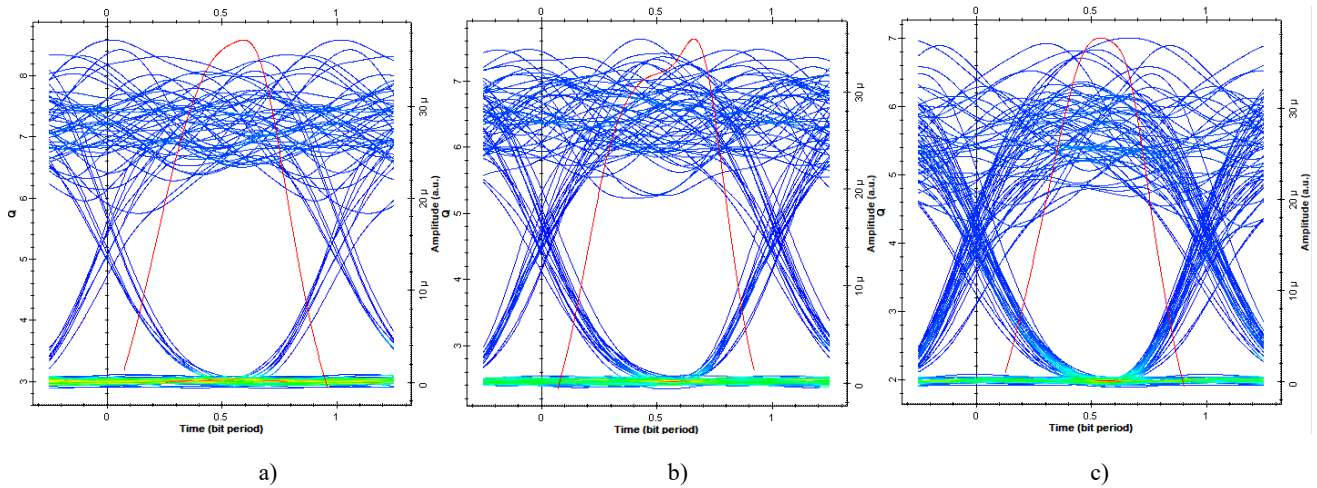


Fig. 17. Eye diagram for NL\_PS at a distance of 50 m varies across different data rates (a) 2.5 Gigabit per second (b) 5 Gigabit per second (c) 10 Gigabit per second (colour online)

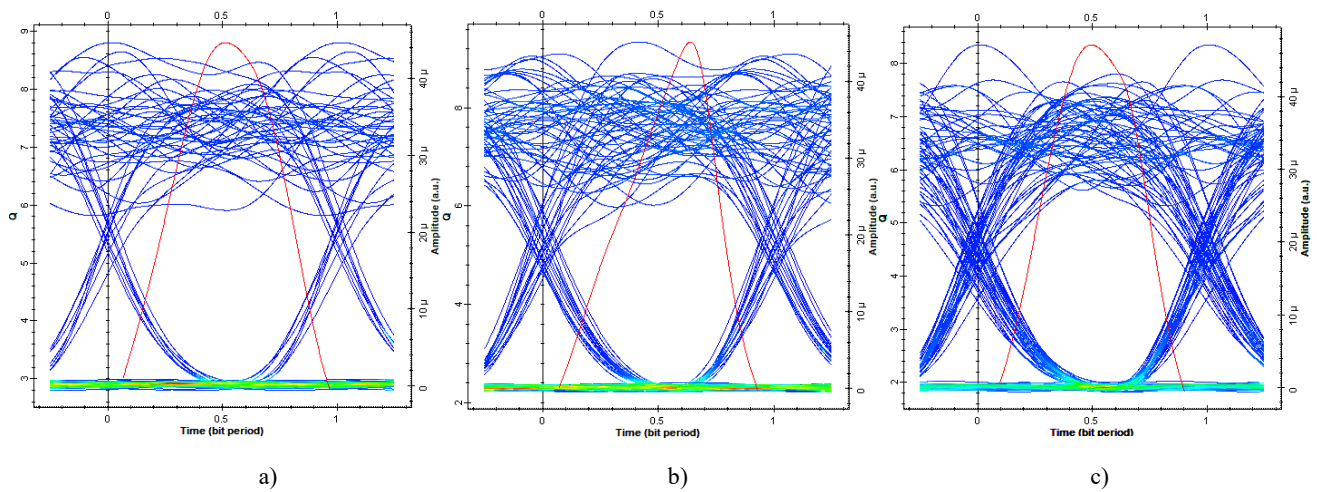


Fig. 18. Eye diagram for NL\_CL at a distance of 50 m varies across different data rates (a) 2.5 Gigabit per second (b) 5 Gigabit per second (c) 10 Gigabit per second (colour online)

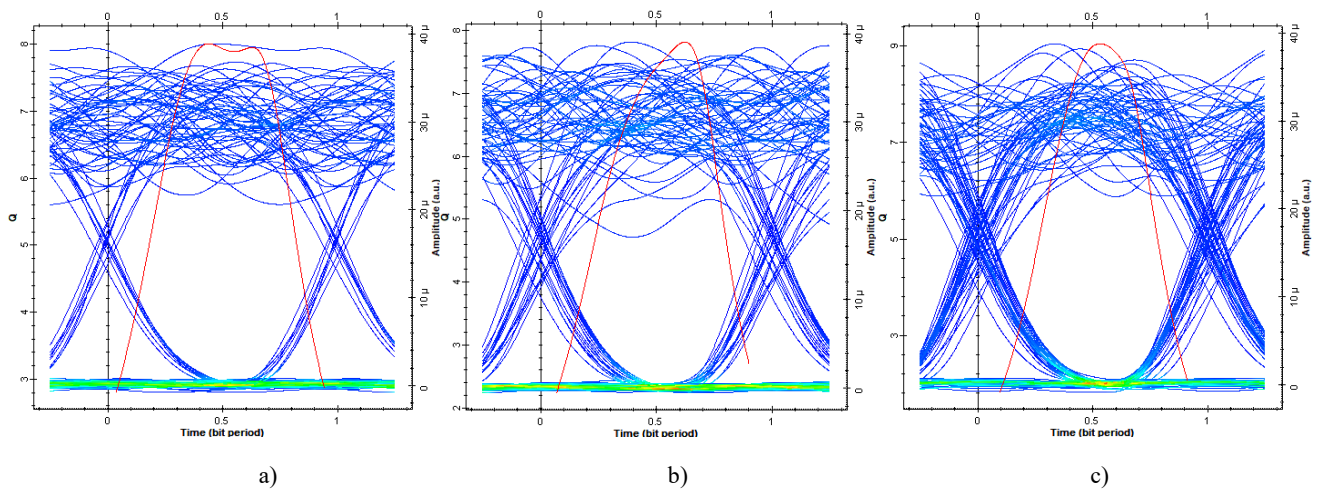


Fig. 19. Eye diagram for NL\_CO at a distance of 50 m varies across different data rates (a) 2.5 Gigabit per second (b) 5 Gigabit per second (c) 10 Gigabit per second (colour online)

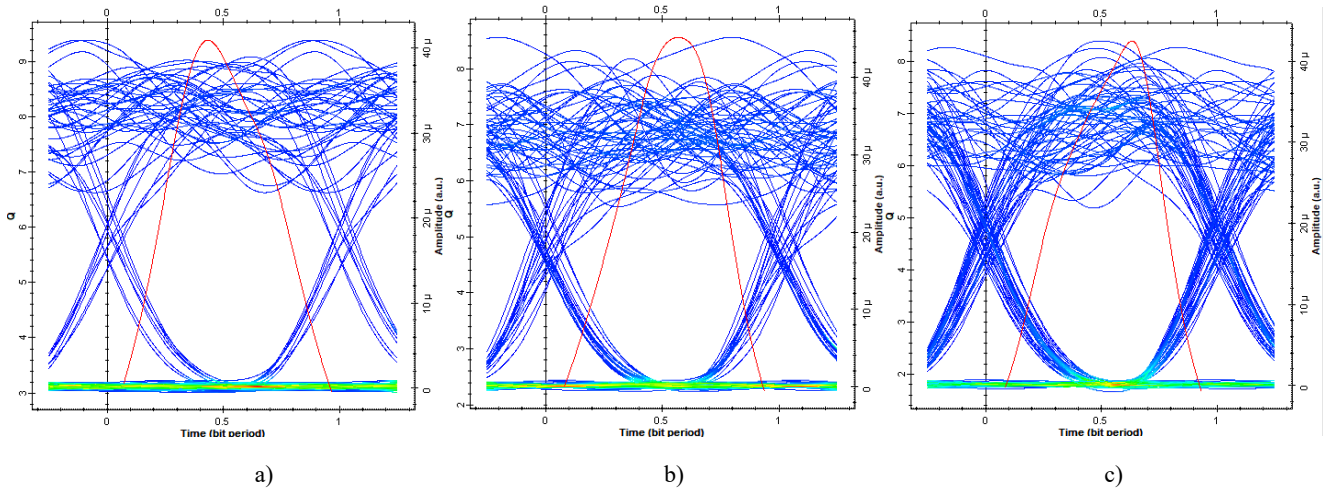


Fig. 20. Eye diagram for NL\_H1 at a distance of 50 m varies across different data rates (a) 2.5 Gigabit per second (b) 5 Gigabit per second (c) 10 Gigabit per second (colour online)

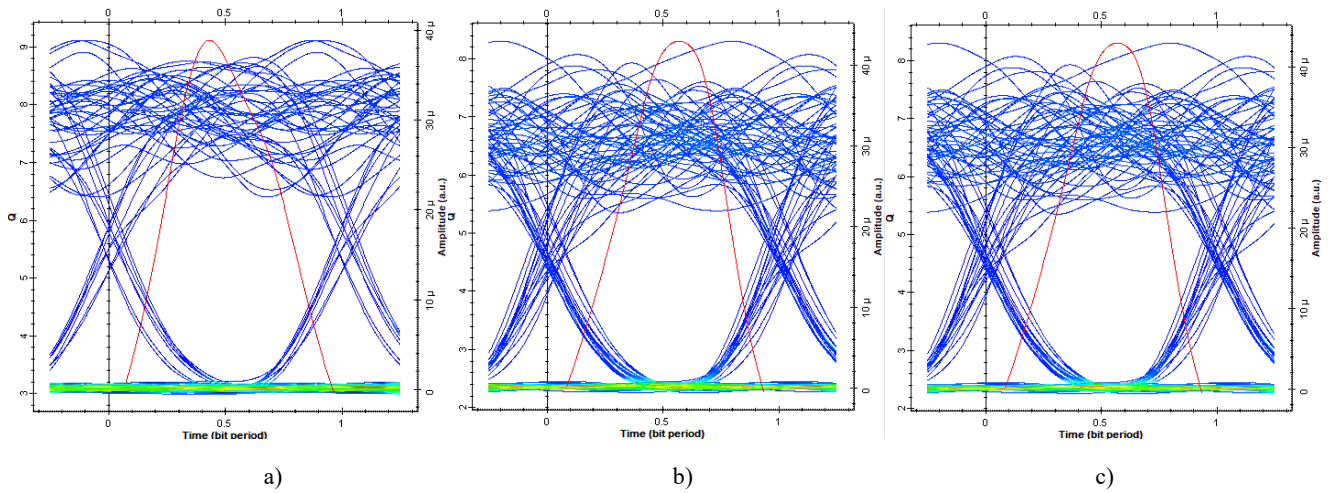


Fig. 21. Eye diagram for NL\_H2 at a distance of 50 m varies across different data rates (a) 2.5 Gigabit per second (b) 5 Gigabit per second (c) 10 Gigabit per second (colour online)

#### 4.4. Comparison of proposed OCDMA based UOWC using Li-Fi with existing work

The comparative analysis of proposed OCDMA based UOWC using Li-Fi with previous literature is shown in Table 4. The five types of waterbodies such as L\_PS, L\_CL, L\_CO, L\_H1, L\_H2 and NL\_PS, NL\_CL, NL\_CO, NL\_H1, NL\_H2 for five channels have been studied in this work.

The 1 Gigabit per second channel capacity for harbor water type with used specifications such as 532 nm wavelength, 12 m distance 30 dBm transmitted power is

achieved by Hameed et al., 2023 [23]. The 50 Gigabit per second overall capacity has been achieved in the present work for 532 nm wavelength, 17.5 m distance for LOS, and 8 m distance for NLOS with transmitted power 15 dBm. The present work shows a 66.6% improvement in overall capacity with longer transmitted distance for LOS and NLOS scenarios for all water types with respect to work done by El-Mottaleb et al., 2023 [6]. Similarly, 25% enhancement has been observed in overall channel capacity with larger distance transmission for both scenarios as compared to research work reported by El-Mottaleb et al., 2023 [8].

Table 4. Comparative analysis of proposed work with previous literature

References	Light Source & (Operating wavelength)	Transmitted Power	Modulation Technique	Water Types & (Range)	Overall Capacity & (No. of Channels)	
Oubei et al. (2015) [24]	LD (520 nm)	NA	NRZ-OOK	Water tank (7 m)	2.3 Gbps (NA)	
Shen et al. (2016) [25]	LD (450 nm)	17.1 dBm	NRZ-OOK	Water tank (20 m)	1.5 Gbps (NA)	
Liu et al. (2017) [26]	LD (520 nm)	50 dBm	NRZ-OOK	Water tank (34.5 m)	2.70 Gbps (NA)	
Ali & Rahi (2018) [27]	LED	7 dBm & 10 dBm	NRZ-OOK & M-PPM	PS (31 m) CS (14 m)	10 Mbps (NA)	
Al Hammadi & Islam (2020) [28]	LD (532 nm)	26.99 dBm	OCDMA/OOC Code	PS (27.9 m) CL (17.1 m)	NA	
Hameed et al. (2023) [23]	LD (532 nm)	30 dBm	Filtered OFDM	Harbor (12 m) Turbid (3 m)	1 Gbps (NA)	
El-Mottaleb et al. (2023) [8]	LD (520 nm)	20 dBm	OCDMA/PV Code	PS (15 m) CL (10 m) CO (5 m)	13.5 Gbps (3)	
Singh et al. (2023) [10]	LD (532 nm)	NA	OAM	PS (10 m) CL (8 m) CO (6.1 m) HI (3.85 m) HII (2.62 m)	40 Gbps (4)	
El-Mottaleb et al. (2023) [6]	LD (532 nm)	15 dBm	OCDMA/DPS Code	PS (13 m) CL (10 m) CO (7.2 m) HI (4.3 m) HII (3 m)	30 Gbps (3)	
Present Work	LD (532 nm)	15 dBm	OCDMA/DPS Code	L_PS (50 m) L_CL (47 m) L_CO (32 m) L_H1 (17.5 m) L_H2 (10 m)	NL_PS (38 m) NL_CL (28 m) NL_CO (12 m) NL_H1 (8 m) NL_H2 (7 m)	50 Gbps (5)

## 5. Conclusion

The comprehensive analysis of an OCDMA based UOWC system using Li-Fi technology, focusing on both LOS and NLOS scenarios across data rates of 2.5, 5 and 10 Gigabit per second has been done in this work. Evaluations conducted in five distinct waterbodies NL\_PS, NL\_CL, NL\_CO, NL\_H1, NL\_H2 and L\_PS, L\_CL, L\_CO, L\_H1, L\_H2 reveal significant variations in Q-Factor performance based on water type and data rate with clear sea (Pure Sea, Clear Ocean, Coastal Ocean) providing the highest Q-Factor and harbor environments the lowest Q-Factor due to higher turbidity and scattering. LOS conditions consistently outperform NLOS, emphasizing the importance of direct optical paths for optimal performance. The present work shows a 66.6% improvement in overall capacity with longer transmitted distance for LOS and NLOS scenarios for all water types with respect to work done [6]. The achieved Q-Factor value at data rate of 2.5 Gigabit per second for LOS scenario in L\_PS is 8.61 with transmitted distance 50 m while in NL\_PS value of Q-Factor that is 8.35 is evaluated

at distance of 38 m. The similar improvement is observed in both scenarios at data rate of 10 Gigabit per second that is Q-Factor of L\_PS (50 m) is 8.18 and NL\_PS (38 m) 8.42. The extracted results Q-Factor of LOS scenario for turbid environment (Harbor 2) are 8.79 and 8.34 at a distance of 10 m for data rate 2.5 and 10 Gigabit per second, respectively. Furthermore, enhanced values of Q-Factor are evaluated in NLOS scenario that is 9.11 and 8.15 with transmitted distance of 7 m at 2.5 and 10 Gigabit per second, respectively. Therefore, the work presents reliable and high data rate communication with required Q-Factor for both scenarios. The wide opening of eye diagrams achieved in this work assure the successful transmission and reception of five underwater channels for both LOS and NLOS systems. Therefore, it is concluded that the proposed work can be used for high speed underwater communication. Furthermore, the advanced modulation schemes, error correction codes and adaptive beamforming can be incorporated with proposed work to enhance system robustness across varying underwater environments and marine based applications.

## Acknowledgement

Gurleen Kaur performed the proposed investigation under the Guidance of Dr. Baljeet Kaur and Dr. Gurburneet Kaur at Guru Nanak Dev Engineering College Ludhiana, India.

## References

- [1] Q. Fu, A. Song, F. Zhang, M. Pan, *IEEE Access* **10**, 38774 (2022).
- [2] H. Y. Ahmed, M. Zeghid, B. Bouallegue, A. Chehri, S. A. Abd El-Mottaleb, *Electronics* **11**(8), 1224 (2022).
- [3] Y. Ata, H. Abumarshoud, L. Bariah, S. Muhaidat, M. A. Imran, *IEEE Photonics Journal* **15**(1), 1 (2023).
- [4] L. Hao, J. Ao, C. Ma, *Cross Strait Radio Science and Wireless Technology (CSRSWTC)*, 13 (2023).
- [5] C. Pallavi, S. Padmaji, *International Journal of Novel Research and Development* **7**, 2456 (2022).
- [6] S. A. A. El-Mottaleb, M. Singh, A. Atieh, A., M. H. Aly, *Optical and Quantum Electronics* **56**(2), 217 (2023).
- [7] G. Kaur, B. Kaur, G. Kaur, *International Journal of Innovative Research in Electrical, Electronics, Instrumentation and Control Engineering (IJIREEIC)* **11**(12), 42 (2023).
- [8] S. A. A. El-Mottaleb, M. Singh, A. Atieh, M. H. Aly, *Optical and Quantum Electronics* **55**(5), 465 (2023).
- [9] R. Salam, A. Srivastava, V. A. Bohara, A. Ashok, *IEEE Open Journal of the Communications Society* (2023).
- [10] M. Singh, S. N. Pottoo, A. Armghan, K. Aliqab, M. Alsharari, S. A. Abd El-Mottaleb, *Applied Sciences* **12**(22), 11374 (2022).
- [11] J. Zhang, X. Wang, B. Wang, W. Sun, H. Du, Y. Zhao, *Sensors* **23**(12), 5759 (2023).
- [12] W. Sahraoui, A. Amphawan, M. B. Jasser, T. K. Neo, *International Journal on Advanced Science, Engineering and Information Technology (IJASEIT)* **13**(6), 2164 (2023).
- [13] G. Schirripa Spagnolo, L. Cozzella, F. Leccese, *Sensors* **20**(8), 2261 (2020).
- [14] S. H. Alnajjar, B. K. ALfaris, *Al-Iraqia Journal for Scientific Engineering Research* **1**(2), 1 (2022).
- [15] N. R. Krishnamoorthy, A. Gerald, G. Rajalakshmi, D. Marshiana, T. T. M. Delsy, *Journal of Physics: Conference Series* **1770**(1), 012030 (2021).
- [16] R. Boluda-Ruiz, P. Rico-Pinazo, B. Castillo-Vázquez, A. García-Zambrana, K. Qaraqe, *IEEE Photonics Journal* **12**(4), 1 (2020).
- [17] N. Venu, A. A. Kumar, *High Technology Letters* **29**, 194 (2023).
- [18] A. Wibisono, M. H. Alsharif, H.-K. Song, B. M. Lee, *IEEE Access* **12**, 34942 (2024).
- [19] R. Karthika, S. Balakrishnan, *SSRG International Journal of Electronics and Communication Engineering* **2**(3), 32 (2015).
- [20] X. Sun, M. Kong, O. Alkhazragi, C. Shen, E. N. Ooi, X. Zhang, B. S. Ooi, *Optics Communications* **461**, 125264 (2020).
- [21] X. Wang, M. Zhang, H. Zhou, X. Ren, *Electronics* **10**(5), 632 (2021).
- [22] C. Fang, S. Li, K. Wang, *IEEE Photonics Journal* **14**(6), 1 (2022).
- [23] S. M. Hameed, A. A. Sabri, S. M. Abdulsatar, *Optical and Quantum Electronics* **55**(1), 77 (2023).
- [24] H. M. Oubei, J. R. Duran, B. Janjua, H. Y. Wang, C. T. Tsai, Y. C. Chi, B. S. Ooi, *Optics Express* **23**(18), 23302 (2015).
- [25] C. Shen, Y. Guo, H. M. Oubei, T. K. Ng, G. Liu, K. H. Park, B. S. Ooi, *Optics Express* **24**(22), 25502 (2016).
- [26] X. Liu, S. Yi, X. Zhou, Z. Fang, Z. J. Qiu, L. Hu, P. Tian, *Optics Express* **25**(22), 27937 (2017).
- [27] M. A. A. Ali, S. K. Rahi, *9th International Symposium on Telecommunications (IST) IEEE*, 270 (2018).
- [28] M. M. Al Hammadi, M. J. Islam, *Photonic Network Communications* **39**(3), 246 (2020).

\*Corresponding author: bansalgurleen98777@gmail.com